Risø–R–1320(EN)

Distance Constant of the Risø Cup Anemometer

Leif Kristensen and Ole Frost Hansen

Risø National Laboratory, Roskilde, Denmark

April 2002

Abstract The theory for cup-anemometer dynamics is presented in some detail, and two methods of obtaining the distance constant $\ell_\circ$ are discussed. The first method is based on wind tunnel measurements: with a constant wind speed the cup anemometer is released from a locked position of the rotor and the increasing rotation rate recorded. It is concluded that the rapid increase in rotation rate makes the method very inaccurate. The second method consists of an analysis of turbulent, atmospheric wind speed as measured by the cup anemometer and a fast-responding sonic anemometer with a spatial eddy resolution, which is significantly better than that which can be obtained by a cup anemometer. The ratio between the measured power spectra of the horizontal wind speed by the two instruments contains the necessary information for determining the response characteristics of the cup anemometer and thereby $\ell_\circ$. The conditions for this last method to be accurate are discussed. Field measurements are used to demonstrate how $\ell_\circ$ is determined for the Risø cup anemometer, model P2546.

ISBN 87–550–3003–3; ISBN 87–550–3004–1 (Internet)
ISSN 0106–2840

Print: Pitney Bowes Management Services Denmark 2002

Contents

1 Introduction

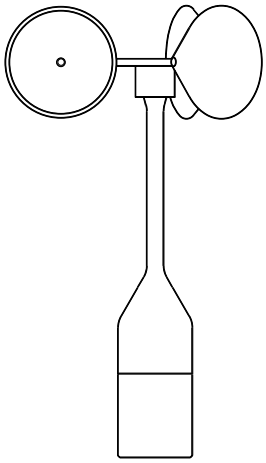

Figure 1. The Risø P2546 anemometer.

The Risø cup anemometer, shown in Fig. 1 has been designed to operate in temperature environments between $-35°$C and $+65°$C and at wind speeds up to 70 m s^{-1}. Its calibration has been shown to be linear up to 20 m s^{-1} to such an extent that the non-linearity is almost undetectable if the wind speed is more than about two meters per second. Wind-tunnel calibrations show that for constant wind speed U the constant rotor angular velocity S in rad s^{-1} is given by

$$S = (U - U_\circ)/\ell, \tag{1}$$

where $\ell \simeq 0.2$ m is the *calibration distance* and $U_\circ \simeq 0.2$ m s^{-1} the *starting speed*. However, it should be emphasized that the linear calibration breaks down when the wind speed is smaller than about 1 m s^{-1}. Neglecting $U_\circ$, the calibration length can be interpreted as the length of air which has to go through the anemometer to have it turn one radian.

The diameter of the conical cups in the three-cup rotor is 7 cm. The cup material is glass-fiber reinforced polycarbonate. The body is made of anodized aluminum. The height of the instrument from the bottom to the center of the rotor is 24.8 cm. The output signal, generated by a magnetically activated switch, is a train of electric pulses, two for each rotor revolution. The wind speed is measured by detecting the rate of these pulses or, alternatively, by measuring the time between every other pulse.

The purpose of this study is to determine how rapidly the instrument reacts to a change in the wind speed when it is exposed to the fluctuating, turbulent wind in open-air environments. This is important to know because the fluctuations in the mean-wind direction may cause *overspeeding*, which can be quantified with this knowledge as shown by Kristensen (1998). Also, if the cup anemometer is used to measure turbulent spectra, the instrument response characteristics must be know.

In the following, we discuss how to specify the response and how to determine it experimentally.

2 Cup Anemometer Dynamics

The equation of motion of the rotation of the cup-anemometer rotor can in general be written (Kristensen 1998)

$$\dot{s}(t) \equiv \frac{\mathrm{d}s}{\mathrm{d}t} = F(s(t), u(t)), \tag{2}$$

where $s(t)$ and $u(t)$ are the instantaneous values of the rate of rotation and wind speed, respectively. Here, we have neglected the lateral and the vertical components in order to simplify the analysis. The response $s(t)$ is to be understood as the running, unweighted average over one full rotation of the cup rotor. This represents the best temporal resolution since, as shown by Coppin (1982), the rotation in general is quite uneven so that a higher sampling rate will cause the signal to fluctuate in a way which does not correctly reflect the real wind-speed fluctuations.

When the anemometer is exposed to the constant laminar wind speed U of a shear-free wind tunnel $s(t)$ becomes constant and equal to S. The calibration of the instrument is determined by means of (2) by substituting $u(t) = U$ and $s(t) = S$. We get

$$0 = F(S, U) \tag{3}$$

which, of course, has the solution (1).

Expanding (2) to the first order in the neighborhood of $(s(t), u(t)) = (S, U)$ leads to

$$\dot{s}(t) = F_1'(S,U)(s(t) - S) + F_2'(S,U)(u(t) - U), \tag{4}$$

where $F_n'(S,U)$ is the partial derivative with respect to argument number n in the point $(s(t), u(t)) = (S, U)$. We observe that in this approximation the cup anemometer is a first-order filter for small excursions in $(s(t) - S, u(t) - U)$. The implication is that $F_1'(S,U)$ must be negative, since it is minus the reciprocal of the time constant $\tau_\circ$ of this filter. If $F_1'(S,U)$ were positive the steady state around the point $(s(t), u(t)) = (S, U)$ could not be maintained. There is a relation between $F_1'(S,U)$ and $F_2'(S,U)$ which can be determined by differentiating (3) with respect to U with S as a function of U given by (1). We get

$$0 = F_1'(S,U)\,\frac{\mathrm{d}S}{\mathrm{d}U} + F_2'(S,U) = \frac{1}{\ell}\,F_1'(S,U) + F_2'(S,U). \tag{5}$$

This means that the equation (4) for small perturbations can be written

$$\dot{s}(t) + \frac{s(t) - S}{\tau_\circ} = \frac{u(t) - U}{\ell\,\tau_\circ}. \tag{6}$$

The right-hand side of (2)—the forcing—which is proportional to the torque on the rotor, is assumed to be a homogeneous second-order polynomial in $s(t)$ and $u(t) - U_\circ$. Since S and U are assumed proportional we see $\tau_\circ$ becomes proportional to $(U - U_\circ)^{-1}$, since

$$\tau_\circ = -\frac{1}{F_1'(S,U)} \propto \frac{1}{U - U_\circ} \tag{7}$$

Consequently,

$$\ell_\circ = (U - U_\circ) \times \tau_\circ \tag{8}$$

is a length which is independent of wind speed and which characterizes the first-order response of the cup anemometer to small perturbations. This length is called the *distance constant*, which is an important instrument constant. We want to discuss two experimental methods for its determination.

Kristensen (1998) postulated a semi-empirical model for the forcing which included $\ell_\circ$ as well as the calibration distance ℓ. In its simplest form it is

$$F(s,u) = \frac{(u - U_\circ - \ell\, s)(u - U_\circ + \beta\ell\, s)}{\ell_\circ\, \ell\, (1+\beta)}, \tag{9}$$

where β, according to Wyngaard et al. (1974) and Coppin (1982), is a never-negative, dimensionless constant.

3 The Wind-Tunnel Method

We consider a situation where the cup anemometer is being calibrated in a wind tunnel. The wind speed is constant and equal to U. The rotor is kept still until time $t = 0$ when it is released. We want to determine how $s(t)$ changes until it attains the constant value S. Thus, we must solve the differential equation

$$\dot{s}(t) = \frac{(U - U_\circ - \ell s(t))(U - U_\circ + \beta\ell s(t))}{\ell_\circ \ell (1+\beta)} \tag{10}$$

with the initial condition $s(0) = 0$. This is a Ricatti type of differential equation which can be reduced to a Bernoulli differential equation by the substitution

$$s(t) = \frac{U - U_\circ - f(t)}{\ell}. \tag{11}$$

We get

$$\frac{\mathrm{d}f}{\mathrm{d}t} + \frac{U - U_\circ}{\ell_\circ}\, f(t) = \frac{\beta}{1+\beta}\, \frac{1}{\ell_\circ}\, f^2(t), \quad f(0) = U - U_\circ. \tag{12}$$

The solution to (12) is

$$f(t) = (U - U_\circ)\, \frac{1+\beta}{\mathrm{e}^{(U-U_\circ)t/\ell_\circ} + \beta}. \tag{13}$$

Inserting into (11) and applying (1) we obtain

$$s(t) = \frac{U - U_\circ}{\ell}\, \frac{1 - \mathrm{e}^{-(U-U_\circ)t/\ell_\circ}}{1 + \beta\, \mathrm{e}^{-(U-U_\circ)t/\ell_\circ}} = S\, \frac{1 - \exp\left(-\dfrac{\ell}{\ell_\circ}\, St\right)}{1 + \beta\, \exp\left(-\dfrac{\ell}{\ell_\circ}\, St\right)}. \tag{14}$$

We see that only in the case $\beta = 0$ the growth of $s(t)$ corresponds to a first-order filter.

By integrating (14) we may determine the total angle $\varphi(t)$ the rotor has turned as a function of time.

$$\varphi(t) = St + \frac{\ell_\circ}{\ell}\,\frac{1+\beta}{\beta}\,\ln\left(\frac{1+\beta\,\exp\left(-\dfrac{\ell}{\ell_\circ}\,St\right)}{1+\beta}\right). \tag{15}$$

Figs. 2 and 3 show examples of $s(t)$ and $-[\varphi(t)-St]$ as functions of time multiplied by the equilibrium rate of rotation.

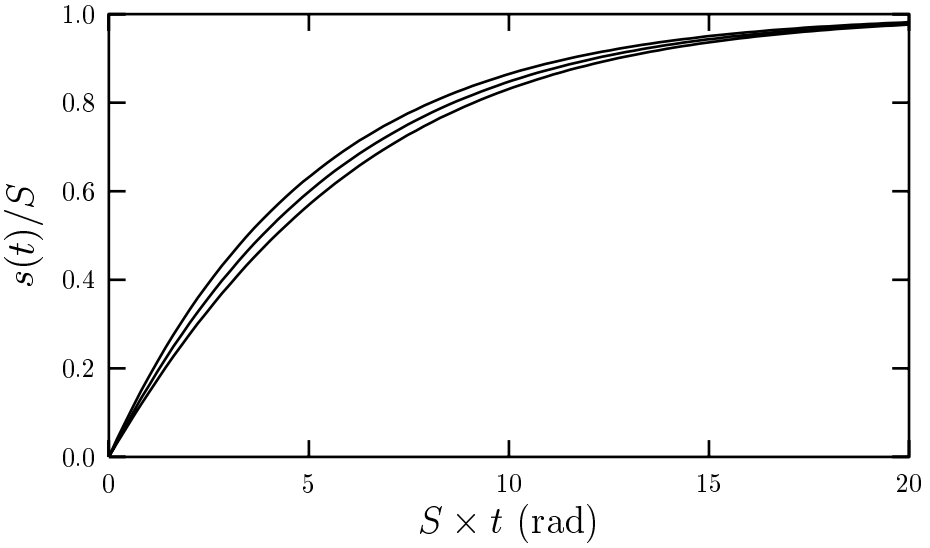

Figure 2. The rate of rotation as a function of dimensionless time for $\ell/\ell_\circ = 0.2$ *and* $\beta = 0.0, 0.15, 0.3$. *The highest curve corresponds to the smallest* β.

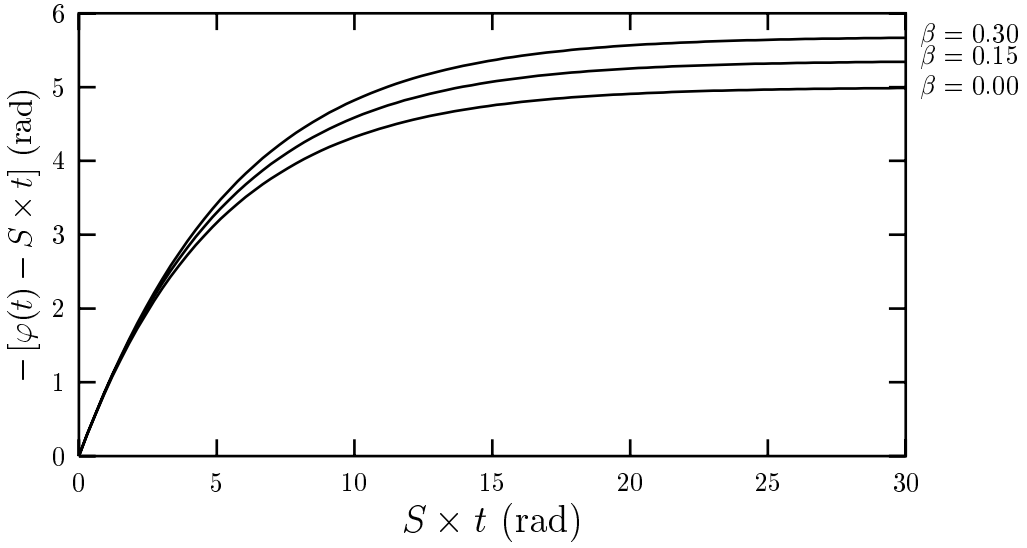

Figure 3. The deficit rotation angle as a function of dimensionless time for $\ell/\ell_\circ = 0.2$ *and* $\beta = 0.0, 0.15, 0.3$.

If the instrument sends one pulse for each full revolution then the number of pulses is

$$n(t) = \frac{S \times (t - t_\circ)}{2\pi} + \frac{1}{2\pi}\,\frac{\ell_\circ}{\ell}\,\frac{1+\beta}{\beta}\,\ln\left(\frac{1+\beta\,\exp\left(-\dfrac{\ell}{\ell_\circ}\,S \times (t - t_\circ)\right)}{1+\beta}\right). \quad (16)$$

Here, only integer values of $n(t)$ are considered. Further, we have allowed for the fact that the first pulse usually appears at a later time than the release time $t_\circ$ of the rotor.

In (16) we know the rate of rotation S for constant wind speed U and of course also the calibration distance ℓ. The unknown parameters are the distance constant $\ell_\circ$, β, and the time of release $t_\circ$. In principle, it should be possible to measure integer pulse numbers $n(t)$ as function of t and then make a fit of (16) to these data to determine the three parameters. However, for the Risø anemometers $\ell_\circ$ is about or slightly larger than $2\pi\ell$. This means that when $n(t)$ exceeds one or two the rotor rotation rate is already constant and close to $S = U/\ell$. The fitting procedure will thus have to be carried out with less than three pairs of $(n(t), t)$. It has been suggested that it should be possible to construct the rotor, such that many more pulses could be emitted from each revolution. This will unfortunately not remedy the situation, since, as pointed out before, the angular velocity within one full revolution is extremely uneven and unpredictable.

4 The Power-Spectrum Method

An alternative to wind-tunnel measurements is to measure atmospheric turbulence with the cup anemometer. If the real turbulence characteristics of the atmosphere is known, it will be possible to determine how rapid the instrument responds fluctuations in term of the time constant $\tau_\circ$ or rather the wind-speed independent distance constant $\ell_\circ$.

In this section, we will first, in order to set the stage, re-develop the statistical tools, i.e. basic Fourier spectral analysis and the transfer function concept. Then, we show how it is possible to obtain information about the "real turbulence" by means of a sonic anemometer. There will be a discussion about the limitations when using discrete, finite Fourier tranforms. Finally, we analyze real atmospheric wind-speed data obtained from simultaneous measurements of the same turbulent fields with a cup anemometer and a sonic anemometer.

4.1 Basic Statistics

We consider the fluctuating parts of the turbulent velocity field and the cup anemometer response

$$\left\{ \begin{array}{c} u'(t) \\ s'(t) \end{array} \right\} = \left\{ \begin{array}{c} u(t) - U \\ s(t) - S \end{array} \right\}. \quad (17)$$

Using angle brackets to indicate averaging, the auto-covariance functions are

$$\left\{ \begin{array}{c} R_u(\tau) \\ R_s(\tau) \end{array} \right\} \equiv \left\{ \begin{array}{c} \langle u'(t)u'(t+\tau)\rangle \\ \langle s'(t)s'(t+\tau)\rangle \end{array} \right\} = \int_{-\infty}^{\infty} \left\{ \begin{array}{c} P_u(\omega) \\ P_s(\omega) \end{array} \right\} \mathrm{e}^{\mathrm{i}\omega\tau}\,\mathrm{d}\omega, \tag{18}$$

where

$$\left\{ \begin{array}{c} P_u(\omega) \\ P_s(\omega) \end{array} \right\} = \frac{1}{2\pi} \int_{-\infty}^{\infty} \left\{ \begin{array}{c} R_u(\tau) \\ R_s(\tau) \end{array} \right\} \mathrm{e}^{-\mathrm{i}\omega\tau}\,\mathrm{d}\tau \tag{19}$$

are the power spectra as functions of the angular frequency ω.

With the primed variables of (17) the differential equation (6) takes the form

$$\dot{s}' + \frac{s'}{\tau_\circ} = \frac{u'}{\ell\,\tau_\circ} \tag{20}$$

which, with the initial condition $s'(-\infty) = 0$ has the solution

$$s'(t) = \frac{1}{\ell} \int_0^{\infty} u'(t-t_1)\,\mathrm{e}^{-t_1/\tau_\circ}\,\frac{\mathrm{d}t_1}{\tau_\circ}. \tag{21}$$

Applying this equation to the middle equation of (18), we get, in view of (19),

$$\begin{aligned} R_s(\tau) &= \frac{1}{\ell}\int_0^{\infty} \mathrm{e}^{-t_1/\tau_\circ}\,\frac{\mathrm{d}t_1}{\tau_\circ}\,\frac{1}{\ell}\int_0^{\infty} \mathrm{e}^{-t_1/\tau_\circ}\,\frac{\mathrm{d}t_1}{\tau_\circ}\,\underbrace{\langle u'(t-t_1)u'(t+\tau-t_2)\rangle}_{R_u(\tau-(t_2-t_1))} \\ &= \frac{1}{\ell}\int_0^{\infty} \mathrm{e}^{-t_1/\tau_\circ}\,\frac{\mathrm{d}t_1}{\tau_\circ}\,\frac{1}{\ell}\int_0^{\infty} \mathrm{e}^{-t_1/\tau_\circ}\,\frac{\mathrm{d}t_1}{\tau_\circ}\int_{-\infty}^{\infty} P_u(\omega)\,\mathrm{e}^{\mathrm{i}\omega(\tau-(t_2-t_1))}\,\mathrm{d}\omega \\ &= \int_{-\infty}^{\infty} P_u(\omega)\,\mathrm{e}^{\mathrm{i}\omega(\tau)}\,\mathrm{d}\omega \left| \frac{1}{\ell}\int_0^{\infty} \exp\left(-\left(\frac{1}{\tau_\circ} - \mathrm{i}\,\omega\right)t\right)\,\frac{\mathrm{d}t}{\tau_\circ}\right|^2 \\ &= \frac{1}{\ell^2}\int_{-\infty}^{\infty} \frac{P_u(\omega)}{1+\omega^2\tau_\circ^2}\,\mathrm{e}^{\mathrm{i}\omega\tau}\,\mathrm{d}\omega. \end{aligned} \tag{22}$$

Inserting (22) into the lower equation (19) yields

$$P_s(\omega) = \frac{1}{\ell^2}\,\frac{P_u(\omega)}{1+\omega^2\tau_\circ^2}. \tag{23}$$

We introduce the transfer function by

$$\mathcal{L}(\omega) \equiv \frac{\ell^2\,P_s(\omega)}{P_u(\omega)} = \frac{1}{1+\omega^2\tau_\circ^2} \tag{24}$$

and see that if we know the spectrum of the unfiltered signal $u'(t)$, we can obtain the time constant $\tau_\circ$ or, if we rewrite (24) with the aid of (8),

$$\mathcal{L}(\omega) = \frac{1}{1+\ell_\circ^2\,(\omega/U)^2} \tag{25}$$

the distance constant $\ell_\circ$.

The variable ω/U is, according to Taylor's hypothesis for frozen turbulence, equal to the wave-number component k_1 in the direction of the mean flow. Consequently, the cup anemometer can be considered a streamwise line filter characterized by the length $\ell_\circ$.

4.2 The Sonic Anemometer

The most common sonic anemometer measures three components of the wind with a temporal resolution better than 0.1 s. For each of these components, the speed of sound is measured almost simultaneously for sound pulses traveling in opposite directions over a path of certain length ℓ^s, which is typically 0.15 m. From the times of flight t_+ and t_- the wind speed component, which can be both positive and negative, is obtained by $(1/t_- - 1/t_+) \times \ell^s$. In this way, the sonic performs an unweighted line averaging of each component over the distance ℓ^s.

We want to determine the spatial sonic filtering of atmospheric turbulence, and since the outer length scale at the altitude z is at least $0.5 \times z$ (Kristensen et al. 1989), i.e. much larger than ℓ^s in cases of practical importance, the atmospheric turbulence may be considered isotropic. Instead of a covariance function for one velocity component, we consider the covariance tensor in three dimensions

$$R_{ij}(\boldsymbol{r}) = \langle u_j(\boldsymbol{x})\, u_j(\boldsymbol{x}+\boldsymbol{r})\rangle, \quad i,j = 1,2,3, \tag{26}$$

where, in a Cartesian coordinate system described by the unit vectors $\boldsymbol{i}_1, \boldsymbol{i}_2, \boldsymbol{i}_3$, $i = 1$ corresponds to the mean-flow direction, $i = 2$ and $i = 3$ to the lateral and the vertical direction, respectively. According to Taylor's hypothesis, the longitudinal lag r_1 is the same as the mean wind speed times the time lag, i.e. $U \times \tau$.

The Covariance tensor can be written in terms of the spectral tensor $\Phi^\circ_{i,j}(\boldsymbol{k})$ as an integral over the entire wave-number space

$$R_{ij}(\boldsymbol{r}) = \int_{\infty} \Phi^\circ_{ij}(\boldsymbol{k})\, \mathrm{e}^{\mathrm{i}\boldsymbol{k}\,\cdot\,\boldsymbol{r}}\, \mathrm{d}^3k, \tag{27}$$

where

$$\Phi^\circ_{ij}(\boldsymbol{k}) = \frac{1}{2\pi} \int_{\infty} R_{ij}(\boldsymbol{r})\, \mathrm{e}^{-\mathrm{i}\boldsymbol{k}\,\cdot\,\boldsymbol{r}}\, \mathrm{d}^3r. \tag{28}$$

When the turbulence is isotropic this tensor is a very simple expression, namely

$$\Phi^\circ_{ij}(\boldsymbol{k}) = \frac{E(k)}{4\pi\, k^2} \left\{ \delta_{il} - \frac{k_i k_j}{k^2} \right\}, \tag{29}$$

where δ_{ij} is the Kronecker delta, $k = \sqrt{k_1^2 + k_2^2 + k_3^2}$ the magnitude of the wave-number vector $\boldsymbol{k}$, and $E(k)$ the energy spectrum which, integrated over k from 0 to ∞ is equal to the specific kinetic energy of the turbulence.

The line averaging along the line

$$\boldsymbol{\ell}^s = \ell^s_1 \boldsymbol{i}_1 + \ell^s_2 \boldsymbol{i}_2 + \ell^s_3 \boldsymbol{i}_3, \quad \ell^s = |\boldsymbol{\ell}^s| \tag{30}$$

corresponds to a filtered spectral tensor of the form

$$\Phi_{ij}(\boldsymbol{k}) = \Phi^{\circ}_{ij}(\boldsymbol{k}) \operatorname{sinc}^2\left(\frac{\boldsymbol{k}\cdot\boldsymbol{\ell}^s}{2}\right), \tag{31}$$

where, by definition,

$$\operatorname{sinc} x = \frac{\sin x}{x}. \tag{32}$$

Here, we are only interested in the turbulent fluctuations of the velocity in the mean-flow direction for which the tensor component is

$$\Phi_{11} = \frac{E(k)}{4\pi\, k^4}\left(k_2^2 + k_3^2\right) \operatorname{sinc}^2\left(\frac{\boldsymbol{k}\cdot\boldsymbol{\ell}^s}{2}\right). \tag{33}$$

We obtain the one-dimensional spectrum $F(k_1)$ along the flow direction by integrating over k_2 and k_3. Since the tensor is axisymmetric with respect to the flow direction we can, without loss of generality let $\ell_3 = 0$ and get

$$F(k_1) = \int_{-\infty}^{\infty} \mathrm{d}k_2 \int_{-\infty}^{\infty} \mathrm{d}k_3 \frac{E(k)}{4\pi\, k^4}\left(k_2^2 + k_3^2\right) \operatorname{sinc}^2\left(\frac{k_1\ell_1^s + k_2\ell_2^s}{2}\right). \tag{34}$$

It is practical to transform the integration variables to plane, polar variables according to

$$\left\{ \begin{array}{c} k_2 \\ k_3 \end{array} \right\} = K \left\{ \begin{array}{c} \cos\Theta \\ \sin\Theta \end{array} \right\} \tag{35}$$

and, in order to ease the notation, to replace k_1 by k. This leads to

$$F(k) = \int_0^{\infty} \frac{E\left(\sqrt{k^2+K^2}\right)}{4\pi\,(k^2+K^2)^2} K^3 \mathrm{d}K \int_0^{2\pi} \operatorname{sinc}^2\left(\frac{k\ell_1^s + K\ell_2^s\cos\Theta}{2}\right) \mathrm{d}\Theta. \tag{36}$$

In the case where $\ell_2^s = 0$, i.e. when the line averaging is in the flow direction, the double integral is easily reduced to a single integral, since

$$\begin{aligned} F_{\parallel}(k) &= \frac{1}{2}\operatorname{sinc}^2\left(\frac{k_1\ell_1^s}{2}\right) \int_0^{\infty} \frac{E\left(\sqrt{k^2+K^2}\right)}{(k^2+K^2)^2} K^3 \mathrm{d}K \\ &= \frac{1}{2}\operatorname{sinc}^2\left(\frac{k_1\ell_1^s}{2}\right) \int_k^{\infty} E(\kappa)\left(\kappa^2 - k^2\right)\frac{\mathrm{d}\kappa}{\kappa^3}. \end{aligned} \tag{37}$$

In the last expression we have applied the transformation

$$\kappa = \sqrt{k^2 + K^2}. \tag{38}$$

Obviously, since the transfer function is the ratio of the filtered and the unfiltered spectrum ($\ell_1^2 = \ell_2^s = \ell_3^2 = 0$), the longitudinal transfer function becomes

$$\mathcal{L}_{\parallel}(k) = \operatorname{sinc}^2\left(\frac{k\ell_1^s}{2}\right) = \operatorname{sinc}^2\left(\frac{\omega\ell^s}{2\,U}\right). \tag{39}$$

The orientation of $\boldsymbol{\ell}^s$ is usually not along the flow. The angle will for most common three-dimensional sonic anemometers in use be between about 55° and 90°. This implies that the double integral (36) cannot in general be reduced to a simple explicit expression, but must be evaluated numerically. However, there is one more situation where it is possible to obtain a transfer function, namely when $\ell_1^s = 0$, i.e. when $\boldsymbol{\ell}^s$ is perpendicular to the mean flow. The evaluation of (36) can then carried out because we have an explicit expression for $E(k)$: since the eddies we are interested in are much smaller than the outer length scale, we have what is called *locally isotropic turbulence*, and in this case

$$E(k) = \alpha\, \varepsilon^{2/3}\, k^{-5/3}. \tag{40}$$

Here ε is the constant rate of dissipation of specific kinetic energy and $\alpha \simeq 1.7$ the so-called Kolmogorov constant.

Substituting in (36), the laterally averaged, longitudinal spectrum becomes

$$\begin{aligned} F_\perp(k) &= \frac{\alpha\,\varepsilon}{4\pi} \int_0^\infty \frac{K^3\,\mathrm{d}K}{(k^2+K^2)^{17/6}} \int_0^{2\pi} \mathrm{sinc}^{\,2}\left(\frac{K\ell^s\cos\Theta}{2}\right)\,\mathrm{d}\Theta \\ &= \frac{1}{2\pi}\,\alpha\,\varepsilon^{2/3}(\ell^s)^{5/3} \int_0^\infty \frac{s^3\,\mathrm{d}s}{(q^2+s^2)^{17/6}} \int_0^{\pi} \mathrm{sinc}^{\,2}\left(\frac{s\cos\Theta}{2}\right)\,\mathrm{d}\Theta, \end{aligned} \tag{41}$$

where $q = k\ell^s$.

The transfer function for lateral averaging becomes

$$\begin{aligned} \mathcal{L}_\perp(k) = {}& {}_1F_2\left(\frac{1}{2};\frac{1}{6},\frac{3}{2};\left\{\frac{k\ell^s}{2}\right\}^2\right) \\ & - \frac{3}{8}\,\frac{\Gamma(1/6)}{\Gamma(11/6)}\,\left(\frac{k\ell^s}{2}\right)^{5/3} {}_1F_2\left(\frac{4}{3};\frac{11}{6},\frac{7}{3};\left\{\frac{k\ell^s}{2}\right\}^2\right), \end{aligned} \tag{42}$$

where ${}_1F_2(a;b,c;x)$ is a Hypergeometric function.

The two transfer functions $\mathcal{L}_\parallel(k)$ and $\mathcal{L}_\perp(k)$ are displayed in Fig. 4. Transfer functions where the angle between $\boldsymbol{\ell}^s$ and the mean-flow direction must lie between $\mathcal{L}_\parallel(k)$ and $\mathcal{L}_\perp(k)$. Since ℓ^s is about 0.15 m while the cup-anemometer distance constant $\ell_\circ$ is about or more than 10 times larger we have shown for comparison a cup anemometer filter with $\ell_\circ = 10 \times \ell^s$. We see that $\mathcal{L}_\parallel(k)$ and $\mathcal{L}_\perp(k)$ are very close to one until the cup-anemometer filter has decreased by a factor of two. Consequently the ratio between the spectrum measured by the cup anemometer and the sonic spectrum can be considered a good approximation to the cup-anemometer transfer function.

4.3 Discrete Spectrum Analysis

In this section, we discuss the difference between the power spectra defined by continuous, infinite Fourier transformations as described by (18) and (19) and

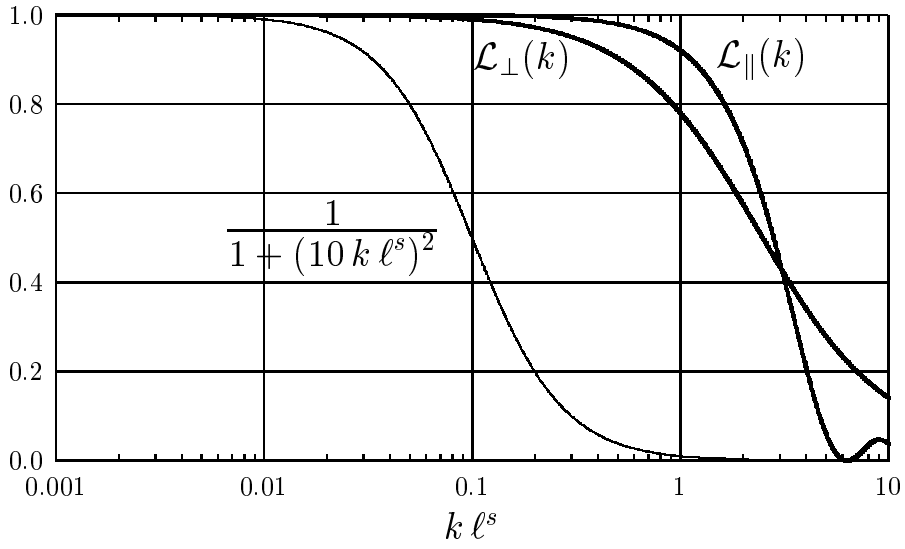

Figure 4. The two sonic transfer functions $\mathcal{L}_\parallel(k)$ and $\mathcal{L}_\perp(k)$ (thick line) as functions of $k\ell^s = \omega\ell^s/U$ and a first-order filter (25) with $\ell_\circ = 10 \times \ell^s$ (thin line).

those obtained by discrete, finite Fourier transformation which since the mid-sixties have been carried out on digital computers by means of the so-called Fast Fourier Transform procedure (FFT).

Let

$$s[n] = s(n\Delta t), \quad n = 0, 1, \ldots, N-1 \tag{43}$$

be the discretely sampled signal from either the sonic anemometer the cup anemometer over the time $T = N\Delta t$, where Δt is the temporal resolution and N the number of points.

The discrete, finite transform of $s[n]$ is, by definition,

$$\widehat{s}[m] = \frac{1}{N}\sum_{n=0}^{N-1} s[n]\,\mathrm{e}^{2\pi\mathrm{i}\,m\,n/N}, \quad m = 0, 1, \ldots, N-1. \tag{44}$$

We immediately see that $\widehat{s}[0]$ is equal to the temporal mean over the time T which, if T is very large, is equal to the ensemble mean S. For $m > 1$, we consider the ensemble average

$$\begin{aligned}
\left\langle |\widehat{s}[m]|^2 \right\rangle &= \left\langle \frac{1}{N}\sum_{n_1=0}^{N-1} s[n_1]\,\mathrm{e}^{2\pi\mathrm{i}\,m\,n_1/N} \frac{1}{N}\sum_{n_2=0}^{N-1} s[n_1]\,\mathrm{e}^{-2\pi\mathrm{i}\,m\,n_2/N} \right\rangle \\
&= \frac{1}{N}\sum_{n_1=0}^{N-1} \mathrm{e}^{2\pi\mathrm{i}\,m\,n_1/N} \frac{1}{N}\sum_{n_2=0}^{N-1} \mathrm{e}^{-2\pi\mathrm{i}\,m\,n_2/N} \underbrace{\langle s[n_1]\,s[n_2]\rangle}_{R_s((n_2-n_1)\Delta t)+S^2} \\
&= \frac{1}{N}\sum_{n_1=0}^{N-1} \mathrm{e}^{2\pi\mathrm{i}\,m\,n_1/N} \frac{1}{N}\sum_{n_2=0}^{N-1} \mathrm{e}^{-2\pi\mathrm{i}\,m\,n_2/N} R_s((n_2-n_1)\Delta t) \\
&\quad + S^2\delta_{0,m},
\end{aligned} \tag{45}$$

where we have used the definitions (17) and (18), (43), and the identity

$$\frac{1}{N}\sum_{n=0}^{N-1} \mathrm{e}^{2\pi \mathrm{i}\, m\, n/N} = \delta_{0,m}. \tag{46}$$

We see that the variance can be obtained by the finite summation

$$\sum_{m=1}^{N-1} \left\langle |\widehat{s}[m]|^2 \right\rangle = \sum_{m=0}^{N-1} \left\langle |\widehat{s}[m]|^2 \right\rangle - \left\langle |\widehat{s}[0]|^2 \right\rangle =$$

$$R_s(0) + S^2 - \left\langle |\widehat{s}[0]|^2 \right\rangle \simeq R_s(0). \tag{47}$$

We return to (45) and consider the interval $1 \leq m \leq N-1$. Substituting (18), we get

$$\begin{aligned} \left\langle |\widehat{s}[m]|^2 \right\rangle &= \int_{-\infty}^{\infty} P_s(\omega)\, \mathrm{d}\omega \left| \frac{1}{N} \sum_{n=0}^{N-1} \exp\Big(\mathrm{i}\, n \left[2\pi \frac{m}{N} - \omega \Delta t\right]\Big) \right|^2 \\ &= \int_{-\infty}^{\infty} P_s(\omega)\, \frac{\sin^2\left(\dfrac{(\omega_m - \omega)T}{2}\right)}{N^2 \sin^2\left(\dfrac{(\omega_m - \omega)T}{2N}\right)}\, \mathrm{d}\omega, \end{aligned} \tag{48}$$

where

$$\omega_m = m\Delta\omega = m\frac{2\pi}{T}. \tag{49}$$

For $N \to \infty$ we have

$$\begin{aligned} D(\omega_m - \omega) &\equiv \frac{\sin^2\left(\dfrac{(\omega_m - \omega)T}{2}\right)}{N^2 \sin^2\left(\dfrac{(\omega_m - \omega)T}{2N}\right)} \\ &\to \mathrm{sinc}^{\,2}\left(\frac{(\omega_m - \omega)T}{2}\right) \to \delta(\omega_M - \omega)\, \Delta\omega, \end{aligned} \tag{50}$$

is Dirac's delta-function. Thus

$$\lim_{N\to\infty} \left[\frac{\left\langle |\widehat{s}[m]|^2 \right\rangle}{\Delta\omega} \right] = \int_{-\infty}^{\infty} P_s(\omega\, \delta(\omega_m - \omega)\, \mathrm{d}\omega = P_s(\omega_m). \tag{51}$$

The exact expression for $D(\omega_m - \omega)$ in (50) shows that this function is equal to unity when

$$\frac{\omega_m - \omega}{2N} T = j \times \pi, \quad j = 0, \pm 1, \pm 2 \ldots. \tag{52}$$

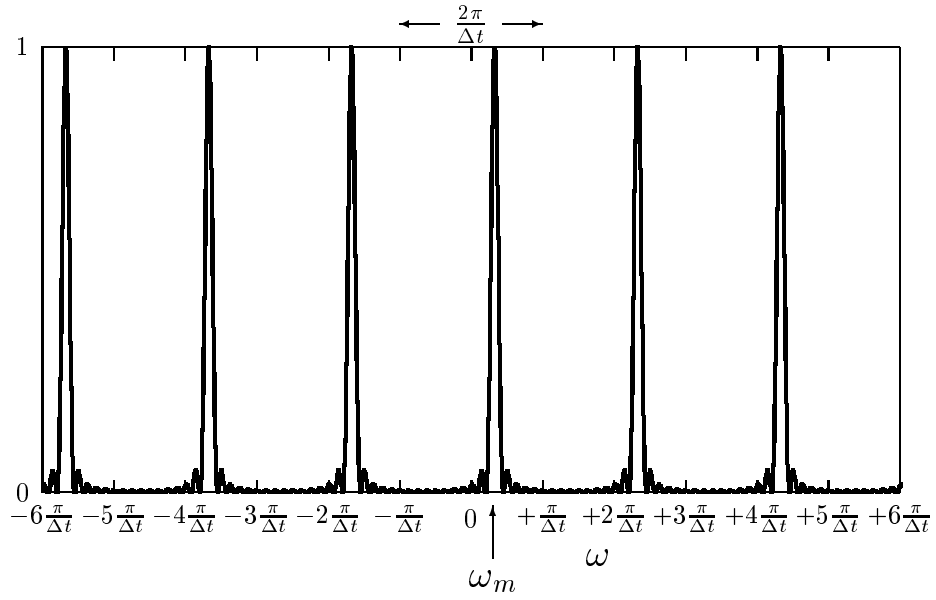

Figure 5. $D(\omega_m - \omega)$ as a function of ω with a fixed, chosen value of ω_m for $N = 16$.

It is periodic in ω with the period $2\pi/\Delta t$ as Fig. 5 shows. This is also the case for $\left\langle |\widehat{s}[m]|^2 \right\rangle$ in ω_m. The aliased spectrum can be considered to lie in the interval $-\pi/\Delta t < \omega_m < \pi/\Delta t$ and, according to (47) containing the entire variance.

When N is very large, 100 say, $D(\omega_m - \omega)$ is well approximated by the so-called *Dirac comb*

$$D(\omega_m - \omega) = \Delta\omega \sum_{j=-\infty}^{\infty} \delta\left(\omega_m - \omega - j\frac{2\pi}{\Delta t}\right). \tag{53}$$

Inserting into (48) we obtain the well-known expression for the *aliased* spectrum

$$P_s^A(\omega_m) \equiv \frac{\left\langle |\widehat{s}[m]|^2 \right\rangle}{\Delta\omega} = \sum_{j=-\infty}^{\infty} P_s\left(\omega_m - j\frac{2\pi}{\Delta t}\right). \tag{54}$$

If the spectrum $P_s(\omega)$ is the filtered sonic spectrum for which the transfer functions are shown in Fig. 4, we conclude aliasing is of no consequence if

$$\frac{\pi}{\Delta t} \gtrsim \frac{U}{\ell^s} \quad \Longleftrightarrow \quad \Delta t \lesssim \pi\frac{\ell^s}{U}. \tag{55}$$

The sonic path length is about $\ell^s = 0.15$ m and the maximum value of U 16 m s^{-1}. To avoid aliasing up to this wind speed, we must consequently demand $\Delta t \lesssim 0.03$ s.

When $s(t)$ represents the cup-anemometer signal, the situation is slightly different. Here, the recording is carried out by means of the so-called *sample-and-hold technique* where the time Δt_i for each full rotor rotation is stored in a register, until it is replaced by the time of the next full rotation. The register is logged at least once for every rotation. The unweighted wind-speed average over one period u_i can then be determined by means of the calibration expression (1), which takes the form

$$u_i = \frac{2\pi\ell}{\Delta t_i} + U_\circ. \tag{56}$$

Figure 6 illustrates the principle.

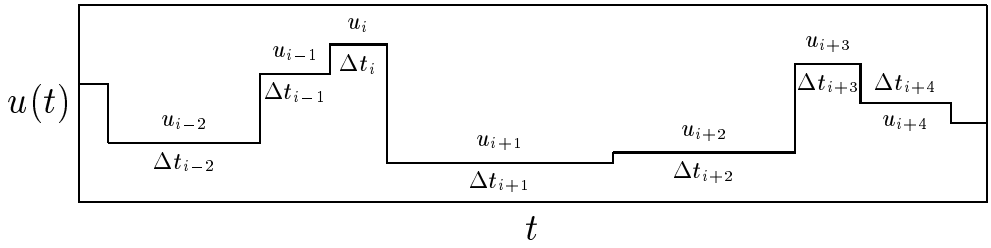

Figure 6. The sample-and-hold technique. We note that in this illustration, where the fluctuations are wildly exaggerated, that smaller values of u_i corresponds, as (56) shows, to larger values of Δt_i.

The wind-speed fluctuations are so small that the rate with which the register is updated may be considered almost constant, within about the relative turbulence intensity. In these considerations we will therefore assume that

$$P_s(\omega) = \mathrm{sinc}^{\,2}\left(\frac{\omega\Delta t}{2}\right) P_s^\circ(\omega) \tag{57}$$

where $P_s^\circ(\omega)$ is the unfiltered cup-anemometer signal.

Inserting into (54), we get in general

$$P_s^A(\omega) = \sum_{j=-\infty}^{\infty} \mathrm{sinc}^{\,2}\left(\frac{\omega\Delta t}{2} - j\pi\right) P_s^\circ\left(\omega - j\,\frac{2\pi}{\Delta t}\right). \tag{58}$$

The transfer function for the averaging in (57) and the aliasing is defined as

$$\mathcal{H}(\omega) = \frac{P_s^A(\omega)}{P_s^\circ(\omega)} \tag{59}$$

which, with the spectral power law

$$P_s^\circ(\omega) = \frac{C}{\omega^p}, \tag{60}$$

can be expressed in terms of well-known functions. We get

$$\begin{aligned}
\mathcal{H}(\omega) &= \sum_{j=-\infty}^{\infty} \mathrm{sinc}^{\,2}\left(\frac{\omega\Delta t}{2} - j\pi\right) \frac{\omega^p}{\left(\omega - j\,\frac{2\pi}{\Delta t}\right)^p} \\
&= \mathrm{sinc}^{\,2}\left(\frac{\omega\Delta t}{2}\right) \left(\frac{\omega\Delta t}{2\pi}\right)^{2+p} \sum_{j=-\infty}^{\infty} \frac{1}{\left(\frac{\omega\Delta t}{2\pi} - j\right)^{2+p}} \\
&= \mathrm{sinc}^{\,2}\left(\frac{\omega\Delta t}{2}\right) \left(\frac{\omega\Delta t}{2\pi}\right)^{2+p} \left\{\zeta\left(2+p, \frac{\omega\Delta t}{2\pi}\right) + \zeta\left(2+p, 1 - \frac{\omega\Delta t}{2\pi}\right)\right\},
\end{aligned} \tag{61}$$

where $\zeta(a, x)$ is the generalized Riemann zeta function.

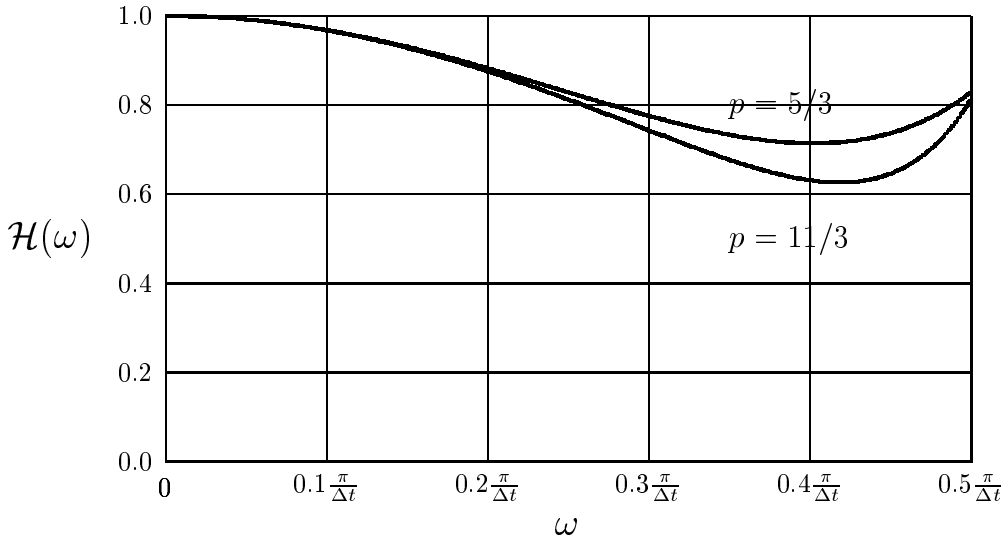

Figure 7. The effect of combined unweighted low-pass filtering and aliasing on turbulent velocities in terms of the transfer function (61).

This transfer function is shown in Fig. 7 for $p = 5/3$ and $p = 11/3$, corresponding to unfiltered and first-order low-pass filtered turbulence.

Here we must compare with the filtering of the cup anemometer with the time constant $\tau_\circ = \ell_\circ/U$. To avoid significant distortion by the sampling procedure, which gives rise to the filtering illustrated by Fig. 7, we demand that $0.2\,\pi/\Delta t \gtrsim 1/\tau_\circ$. Since we have the approximate relation between Δt and the mean-wind speed

$$\frac{2\pi\ell}{\Delta t} \approx U \tag{62}$$

this requirement can be translated into a relation between the distance constant $\ell_\circ$ and the calibration distance ℓ of the cup anemometer. We find that

$$\ell_\circ \gtrsim 10 \times \ell \tag{63}$$

must be fulfilled in order for us to trust the power-spectrum method. The result is not surprising since the sample-and-hold method gives rise to a low-pass filtering characterized by ℓ while the inertia of the rotor results in a low-pass filtering determined by $\ell_\circ$.

4.4 Data Analysis: Distance Constant of the Risø P2546 Anemometer

In the period from 1st of March through 13th of March, 2002, wind speed measurements were carried out at the RIMI (Risø Integrated Milieu* Initiative) a few hundred meters northeast of Risø. The experimental setup is shown in Fig. 8.

A Solent omnidirectional sonic anemometer model 1012SR with the acoustic path length $\ell^s = 0.15$ m was mounted on one boom and a Risø cup anemometer model P2546 on the other. The sampling rate was 20 Hz for both instruments. According to (55) we must require that $U \lesssim \pi\ell^s/\Delta t \simeq 10$ m s^{-1} in order to justify that

*Environment

Figure 8. The RIMI experimental setup as seen from west. The cup anemometer to the far left is the Risø P2546 model. The height of the rotor is 2.2m and the boom is pointing north. The Solent three-dimensional sonic anemometer is mounted on the boom pointing in the direction 240°. The middle of its measuring volume is at the height 2.3 m.

aliasing can be ignored. For the cup anemometer we require that the sampling rate is so high that there is at least one data point for each revolution. Since one revolution takes the time $2\pi \times \ell/U$, and since the standard wind-tunnel calibration (see (1)) for this model is $(U_\circ, \ell) = (0.269 \pm 0.013\,\mathrm{m\,s^{-1}}, 0.19733 \pm 0.0008\,\mathrm{m})$ this requirement means that the wind speed is $U \lesssim 2\pi \times \ell/\Delta t \simeq 25$ m s^{-1} with $\Delta t = 0.05$ s. The sonic anemometer measures the wind speed in three dimensions and to account for wind-direction fluctuation we compare the power spectra of the instantaneous value of the cup anemometer signal with that of the instantaneous value of the total horizontal component as measured by the sonic anemometer.

The data from these 13 days are displayed as half-hour averages in Fig. 9. The lower frame shows that the mean-wind speed never exceeded 10 m s^{-1}. This shows that the above mentioned sampling criteria are met.

The spectra $F^{\mathrm{son}}(k)$ and $F^{\mathrm{cup}}(k)$ of the wind speed as measured by the sonic anemometer and the cup anemometer, respectively, are shown in Fig. 10 in a standard meteorological representation, which would have been area conserving if the ordinate had been linear. Each spectrum was calculated using the FFT routine on the each period in its entire length, and a smoothing with constant relative bandwidth was used on the raw spectral estimates. The spectrum at the lower frequencies, which showed strong fluctuations due to lack of stationarity, were simply left out of the analysis.

All frequencies are transformed into wave numbers according to Taylor's hypothesis: $k = \omega/U$. We note that all the cup-anemometer spectra show a relative maximum at about $k = 1/\ell \simeq 5\,\mathrm{m^{-1}}$. The reason for this maximum is that the signal is over-sampled: referring to Fig. 6, the duration of each step-value is about $2\pi\ell/U$, i.e. 0.25 s at $U = 5\,\mathrm{m\,s^{-1}}$. So with a sampling rate of 20 a constant value will be recorded five times before the value changes. The abrupt change will

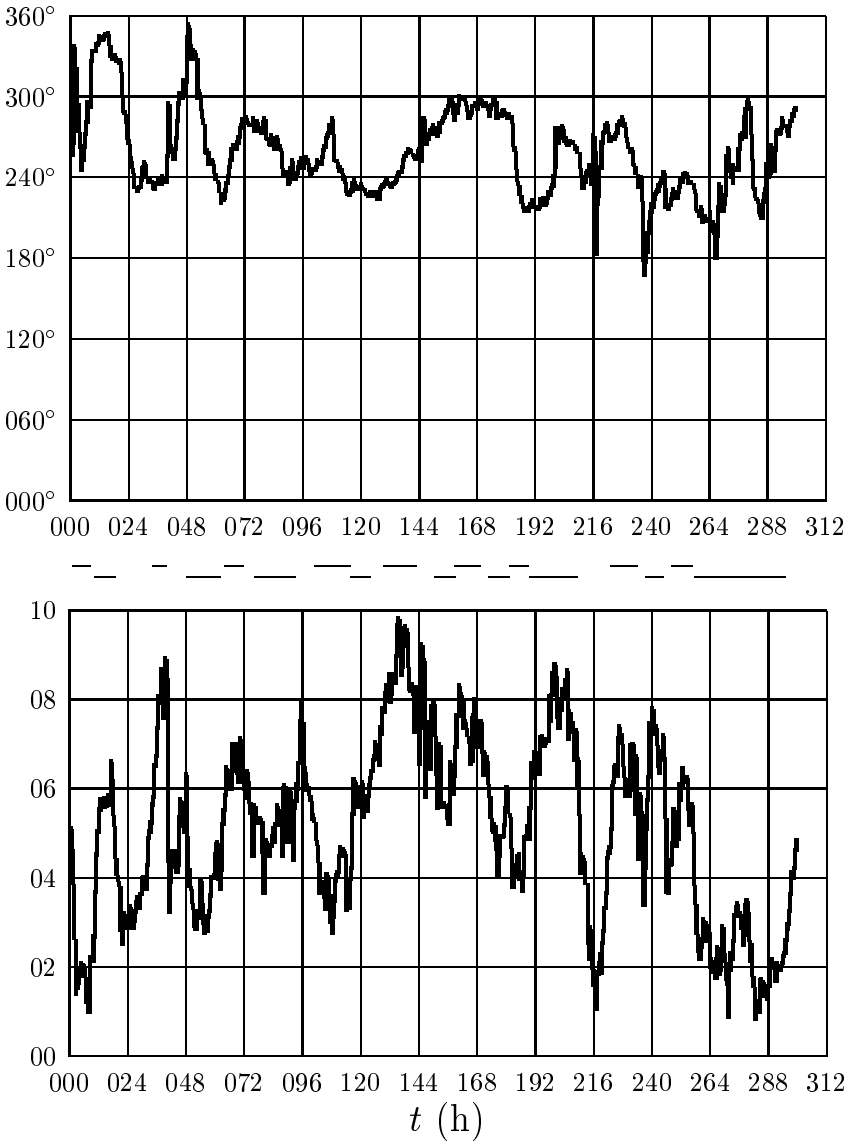

Figure 9. Half-hour averages of the direction (upper frame) and cup-anemometer wind speed (lower frame) as functions of time in hours. The wind direction is almost entirely from south through west to north while the wind speeds lie between 1 and 10 m s^{-1}. The thin lines between the two frames indicate the 18 periods which are analyzed. Their durations are between 5.5 and 37 h.

with this dense sampling cause a transient response around the center frequency $\omega = U/\ell$, i.e. at the wave number $k = \omega/U = 1/\ell$.

The transfer functions

$$\mathcal{H} = \frac{F^{\mathrm{cup}}(k)}{F^{\mathrm{son}}(k)} \tag{64}$$

are shown for all the spectra in Fig. 11.

Since the length scale for the sonic filter is so much smaller than the distance constant of the cup anemometer, we expect that $\mathcal{H}(k)$ will have the form (25) with ω/U replaced by the wave number k. To allow for a possible (small) calibration

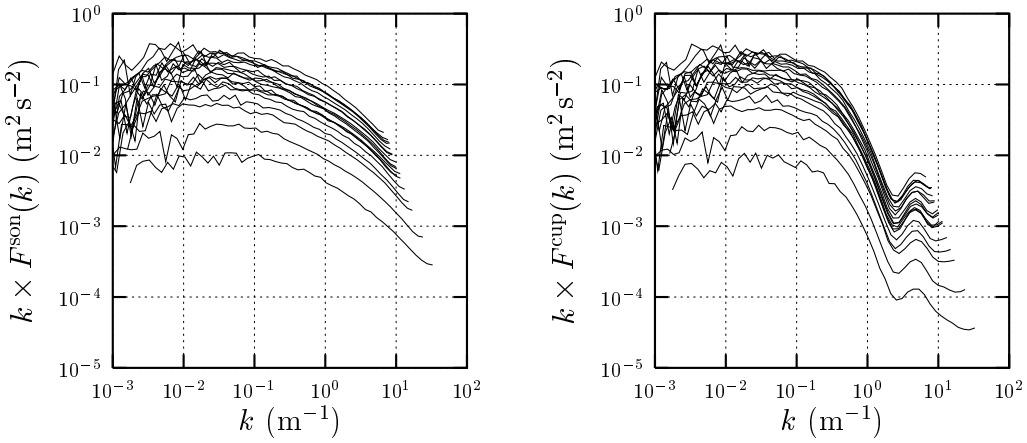

Figure 10. The spectra from the 18 periods as functions of the wave number $k = \omega/U$. There is a very close correspondence between the individual spectra from the sonic (left) and the cup (right).

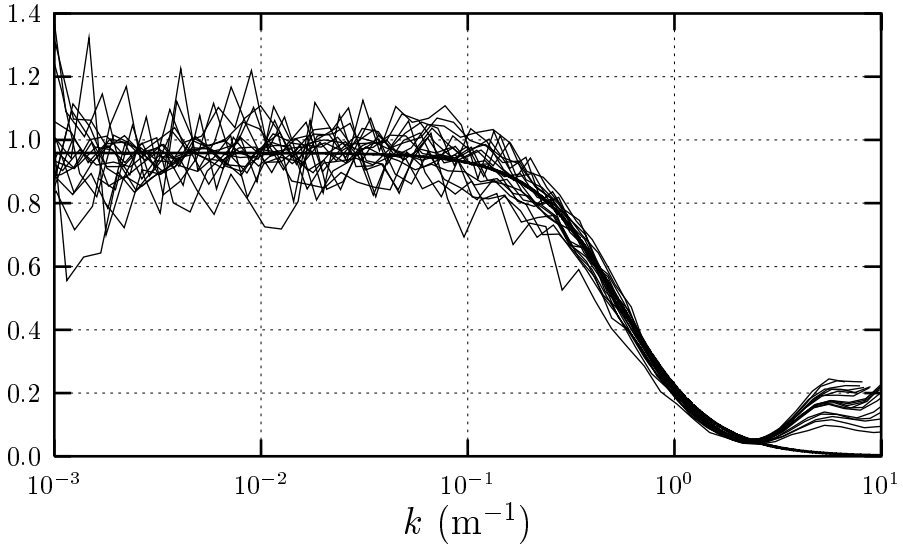

Figure 11. The 18 individual transfer functions (thin lines) and the best common fit (thick line).

discrepancy between the two instrument, we fit each of the transfer functions to

$$\mathcal{H}(k) = \frac{a}{1 + \ell_\circ^2 k^2}, \tag{65}$$

where a is a dimensionless constant. We use the range $10^{-3}\,\mathrm{m^{-1}} < k < 0.5\,\mathrm{m^{-1}}$ and the results are given in Table 1 and Fig. 12. After the fitting, the distance constant was corrected for the effect that the cup-anemometer starting speed $U_\circ$ is different from zero according to the procedure (see (8)

$$\ell_\circ := \frac{U - U_\circ}{U}\,\ell_\circ. \tag{66}$$

We note that a is about 0.95 which means that the sonic anemometer on average measures a 2.5% too high wind speed compared to the cup anemometer.

Table 1. The results of the fitting of the measured transfer functions (64) and the theoretical transfer function (65) in increasing order of the mean-wind speed U.

U (ms^{-1})	$\ell_\circ$ (m)	a
1.76	1.918±0.225	0.878±0.022
2.51	1.871±0.104	0.915±0.009
3.46	1.769±0.119	0.905±0.019
3.93	1.906±0.093	0.928±0.008
4.37	1.887±0.118	0.934±0.011
5.06	1.688±0.143	0.995±0.013
5.11	1.693±0.121	0.985±0.011
5.64	1.812±0.234	0.941±0.020
5.73	1.851±0.096	0.975±0.008
5.83	1.859±0.093	0.951±0.008
5.86	1.655±0.245	0.966±0.022
6.50	1.648±0.174	1.016±0.017
6.57	1.701±0.140	0.982±0.013
6.97	1.940±0.135	1.005±0.012
7.43	1.777±0.089	0.983±0.008
7.51	1.536±0.266	0.944±0.025
7.61	1.649±0.091	0.961±0.008
8.64	1.927±0.076	0.973±0.006
	1.813±0.036	0.951±0.003

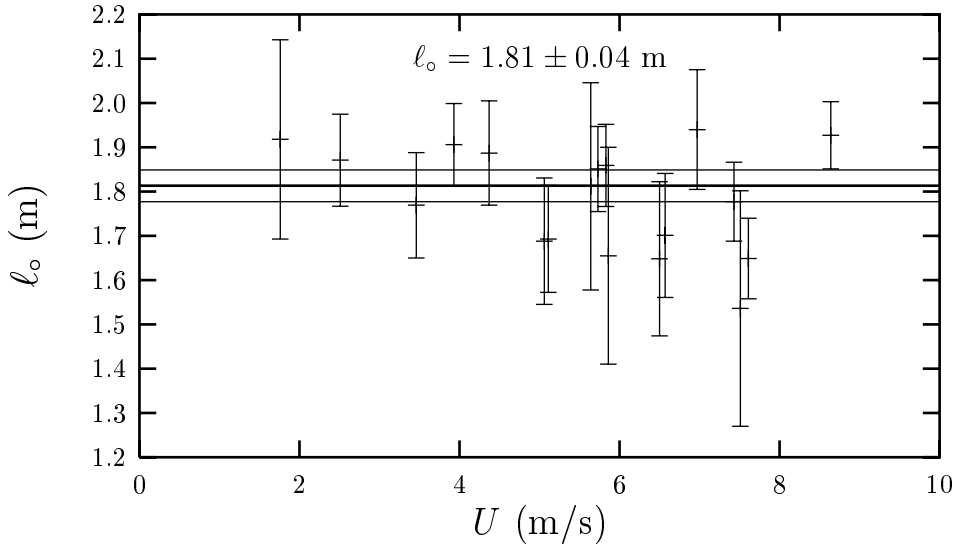

Figure 12. The individual estimates of the distance constant together with the overall, weighted average. The 68% confidence limits are shown.

Figure 12 indicates that there is no apparent dependence of the distance constant $\ell_\circ = 1.81 \pm 0.04$ m on the mean-wind speed. This is a confirmation of the theory that the distance constant is a true instrument constant.

5 Conclusions

The purpose of this investigation has been to describe and test a method of obtaining the distance constant $\ell_\circ$ of a cup anemometer by comparing the power spectrum measured by the cup anemometer and that measured by a sonic anemometer. We have had in the Risø model P2546 particularly in mind, but the method can be applied to other cup anemometers provided $\ell_\circ$ is much larger than the calibration length ℓ and provided the linear dimensions of the sonic spatial averaging is much smaller $\ell_\circ$. We have used the semi-empirical model for cup-anemometer dynamics by Kristensen (1998) as a basis.

First, we discussed theoretically the wind-tunnel method, where there is a constant wind and where the rotor is kept fixed until it is released at a given time. In principle, the signal from the anemometer, the rotor rotation rate, would show an almost exponential increase if the rotation rate were smooth. This, however, is not the case, and only the time for each full rotor rotation can be used for the analysis. Since it takes less than about three full rotations to attain 90% of the equilibrium rotation rate, there will be two few points to fit the almost exponential growth with any confidence and its time constant. Further, the growth from zero to equilibrium rotation rate is not exponential and an extra parameter is needed to describe the growth.

The effects of filtering and aliasing in the data analysis using the comparison method has been discussed and the limits of its applicability established.

Finally, a set of measurements from the RIMI site, where a cup and a sonic operated together for 13 days, has been analyzed. The result from the analysis showed that $\ell_\circ$ is 1.81 ± 0.04 m.

Acknowledgements

We are indebted to our colleagues Kim Pilegaard for his readiness to let us use the RIMI site installation and to Søren W. Lund for his assistance in obtaining the data for the analysis and for photographing the experimental setup.

References

Coppin, P. A. (1982), 'Cup anemometer overspeeding', *Meteorol. Rdsch.* **35**, 1–11.

Kristensen, L. (1998), 'Cup anemometer behavior in turbulent environments', *J. Atmos. Ocean. Technol.* **15**, 5–17.

Kristensen, L., Lenschow, D. H., Kirkegaard, P. & Courtney, M. S. (1989), 'The spectral velocity tensor for homogeneous boundary-layer turbulence', *Boundary-Layer Meteorol.* **47**, 149–193.

Wyngaard, J. C., Bauman, J. T. & Lynch, R. A. (1974), Cup anemometer dynamics, *in* 'Proc. Flow, Its Measurements and Control in Science and Industry', Vol. 1, Instrument Society of America, Pittsburg, PA, pp. 701–708.

Bibliographic Data Sheet **Risø–R–1320(EN)**

Title and author(s)

Distance Constant of the Risø Cup Anemometer

Leif Kristensen and Ole Frost Hansen

ISBN	ISSN
87–550–3003–3; 87–550–3004–1 (Internet)	0106–2840

Dept. or group	Date
Department of Wind Energy	April 30, 2002

Groups own reg. number(s) Project/contract No.

Sponsorship

Pages	Tables	Illustrations	References
25	1	12	4

Abstract (Max. 2000 char.)

The theory for cup-anemometer dynamics is presented in some detail and two methods of obtaining the distance constant $\ell_\circ$ are discussed. The first method is based on wind tunnel measurements: with a constant wind speed the cup anemometer is released from a locked position of the rotor and the increasing rotation rate recorded. It is concluded that the rapid increase in rotation rate makes the method very inaccurate. The second method consists of an analysis of turbulent, atmospheric of wind speed as measured by the cup anemometer and a fast-responding sonic anemometer with a spatial eddy resolution which is significantly better than that which can be obtained by a cup anemometer. The ratio between the measured power spectra of the horizontal wind speed by the two instruments contains the necessary information for determining the response characteristics of the cup anemometer and thereby $\ell_\circ$. The conditions for this last method to be accurate are discussed. Field measurements are used to demonstrate how $\ell_\circ$ is determined the Risø cup anemometer, model P2546.

Descriptors INIS/EDB

WIND; VELOCITY; ANEMOMETER; CALIBRATION; FIELD TESTS; DATA ANALYSIS

Available on request from Information Service Department, Risø National Laboratory (Afdelingen for Informationsservice, Forskningscenter Risø), P.O. Box 49, DK–4000 Roskilde, Denmark.
Phone +45 46 77 40 04, Fax +45 46 77 40 13, E-mail infserv@risoe.dk